Self-Assembled Naphthalimide-Substituted Porphyrin Nanowires for Photocatalytic Hydrogen Evolution

Govardhana Babu Bodedla,[a] *Jun Huang,*[b] *Wai-Yeung Wong,*[c,]* *and Xunjin Zhu*[a,]**

[a] Department of Chemistry and Institute of Advanced Materials, Hong Kong Baptist University, Waterloo Road, Kowloon Tong, Hong Kong, P. R. China.

[b] School of Chemical and Biomolecular Engineering, The University of Sydney, Sydney, Australia.

[c] Department of Applied Biology & Chemical Technology. The Hong Kong Polytechnic University. Hong Kong, P. R. China; The Hong Kong Polytechnic University Shenzhen Research Institute, Shenzhen, 518057, P. R. China.

KEYWORDS. Porphyrins, naphthalimide-conjugation, self-assembly, heterogeneous catalysis, photocatalytic hydrogen evolution

ABSTRACT. A new linear 5,15-di(naphthalimide) substituted porphyrin ZnD(*p*-NI)PP is facilely self-assembled into nanowires in solid with well-defined morphology through the synergistic π-π stack interactions of both porphyrin and naphthalimide skeletons. The self-assembled porphyrin nanowires feature broadened light absorption, efficient separation and transfer of photogenerated charges, and enhanced photostability. As a result, the ZnD(*p*-NI)PP produced 108 times higher H_2

production rate (ηH_2 = 5.4 mmol g^{-1} h^{-1}) than the control 5,15-diphenylporphyrin (ZnDPP) (ηH_2 = 0.05 mmol g^{-1} h^{-1}) and 3.6-fold higher than the ZnT(*p*-NI)PP (ηH_2 = 1.5 mmol $g^{-1}h^{-1}$) which bears four NI units and self-assembled into nanospheres in solid. Moreover, the system of ZnD(*p*-NI)PP continued to show ηH_2 up to 50 h, whereas the system of ZnDPP dropped the ηH_2 after 20 h.

Self-assembled porphyrins and derivatives with well-defined size, shape, and arrangement have gained much attention in optoelectronics, photocatalytic water splitting, pollutants degradation and photodynamic therapy, etc, owing to enhanced visible light capture, generation and separation of photogenerated carriers and reduced charge recombination.[1-7] Generally, the porphyrin derivatives self-assemble by noncovalent interactions such as π–π stacking between the porphyrin rings, ligand coordination, hydrogen bonding of hydroxyl (OH)/carboxylic acid (COOH) groups.[8-10] Self-assembled porphyrin derivatives have been well explored in optoelectronics, pollutants degradation and photodynamic therapy, as well as photocatalytic hydrogen evolution (PHE). Porphyrins as photocatalysts for PHE from water have attracted increasing interest due to their strong light harvesting properties in UV-Visible region, stable excited states, tunable optoelectronic and high thermal stability.[11] Porphyrin-based photocatalysts in bulk synthetic environments usually have undefined morphology. Using such bulk materials for PHE without controlled shape and dimensions could not improve the light-harvesting ability, photogenerated charge-carrier separation and transfers, and consequently reducing PHE. Thus using self-assembled porphyrin derivatives featuring well-defined size, shape and arrangement can enable enhanced visible light capture, exciton diffusion, electron transport and effectively inhibit charge recombination for enhanced PHE. Moreover, porphyrins self-assembling into nanostructured materials with different morphology have not been investigated by tailoring the molecular

structure of porphyrins, which should be an ideal strategy to explore the porphyrin structure-PHE activity relationship. On another side, naphthalimide derivatives have recently been employed as building blocks in metal based supramolecular architectures[12, 13] and aggregation induced emission self-assembled structures.[14, 15] The C=O···π and π···π interactions involving the naphthalimide rings induce supramolecular assembly for the metal complexes and organic derivatives.[12, 14-16] In our previous work, we reported that the star-shaped ZnT(*p*-NI)PP porphyrin containing naphthalimide (NI) moiety (Figure 1) with higher PHE compared to Zinc(II)-tetraphenylporphyrin (ZnTPP).[17] This could be ascribed to efficient intramolecular energy transfer from the NI moiety to the porphyrin ring, which further enhanced the electron transfer from the photo-excited porphyrin moiety to the Pt cocatalyst.

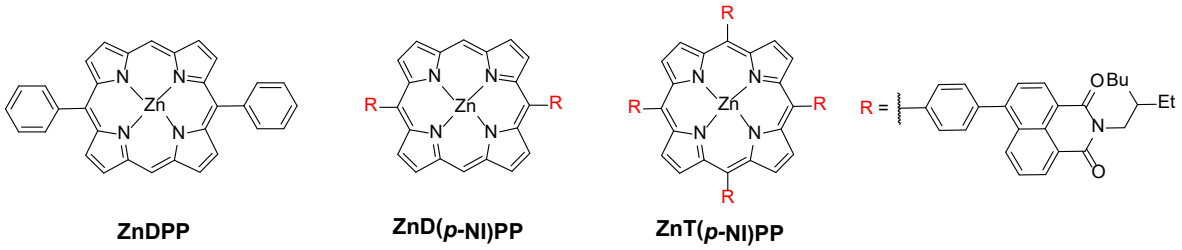

Figure 1. Structures of ZnD(*p*-NI)PP, ZnDPP and ZnT(*p*-NI)PP.

By taking the advantages such as enhancing light harvesting and inducing supramolecular assembly of NI moiety, we herein synthesized a linear-shaped di-NI conjugated porphyrin, ZnD(*p*-NI)PP and compared with the ZnDPP (Figure 1) without NI moieties in terms of morphological, photophysical, electrochemical and PHE properties. We presumed that, as ZnD(*p*-NI)PP containing two NI units with linear-shaped molecular structure, can form more orderly arrangement and morphology in the solid-state than ZnDPP porphyrin due to the strong intermolecular interactions of 5,15-substituted NI moieties, which can directly affect the light-harvesting, photoinduced charge separation and thus PHE performance. In our previous report,[17] though the effect of NI moiety on the PHE performance of the porphyrins was evaluated through

optoelectronic properties in solution, we did not study how the solid-state morphology of the porphyrins plays a role to affect the PHE. Since the heterogeneous PHE performance of porphyrins also largely relay on the morphological properties in solid-state, studying of solid-state morphology of ZnD(*p*-NI)PP combining with optoelectronic properties in solution is worthy to look insight into the heterogeneous PHE process of NI-conjugated porphyrins.

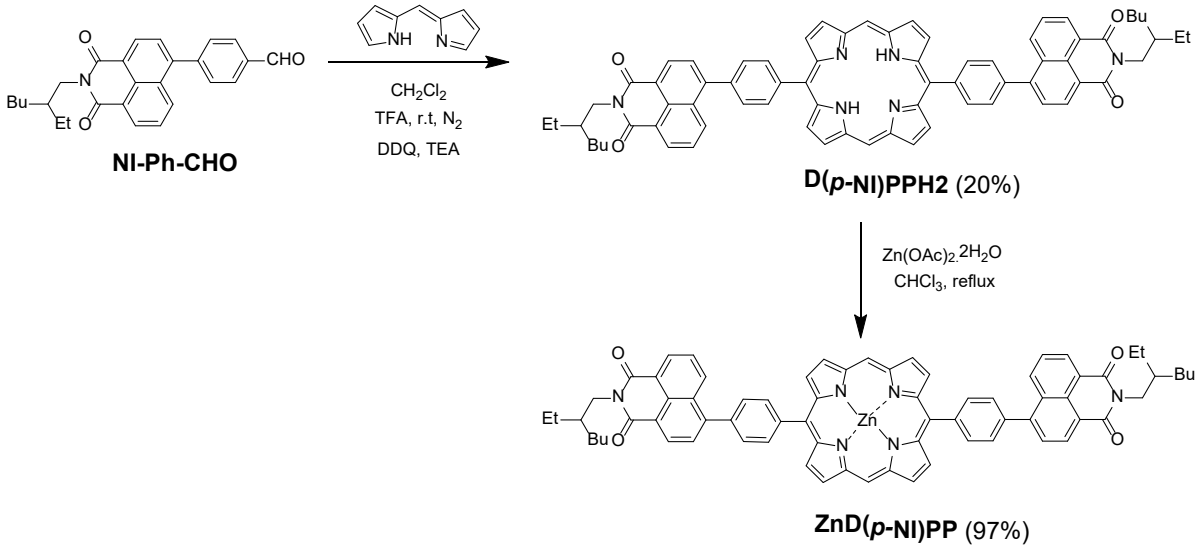

Scheme 1. Synthesis of linear naphthalimide substituted porphyrin, ZnD(*p*-NI)PP.

RESULTS AND DISCUSSION

As illustrated in Scheme 1, the ZnD(*p*-NI)PP was prepared via the reaction of 1-(*para*-formalphenyl)-NI (NI-Ph-CHO) with dipyrromethane in the presence of trifluoroacetic acid, followed by the complexation with $Zn(OAc)_2$ in chloroform ($CHCl_3$). The ZnDPP was prepared for comparison and its synthesis is shown in Scheme S1. Both porphyrins were characterized by nuclear magnetic resonance (NMR) and matrix assisted laser desorption ionization-time of flight mass spectrometry (MALDI-TOF MS) (Supporting Information).

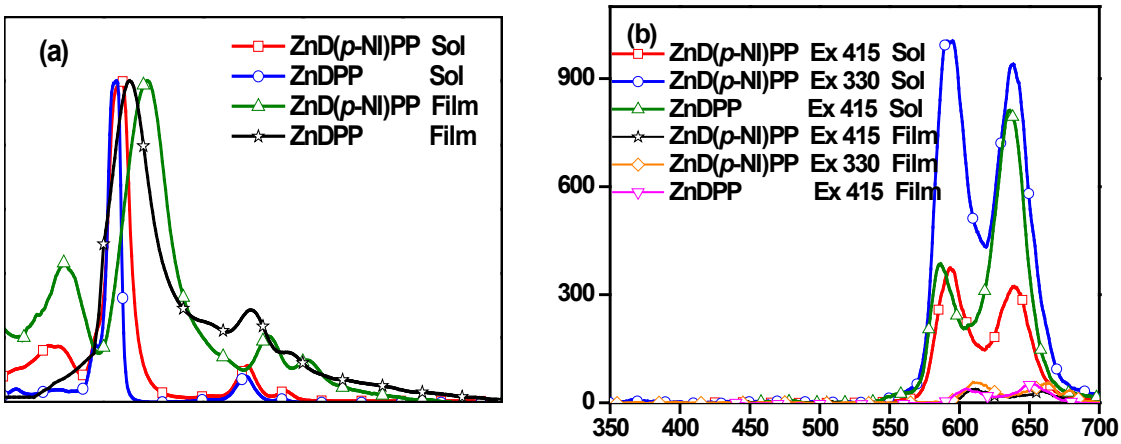

Figure 2. (a) UV-Vis absorption of the porphyrins in THF solution (10 μM) and drop-cast coated thin films (100 μM) at room temperature and (b) Emission spectra of the porphyrins in THF solution (10 μM) and drop-cast coated thin films at room temperature.

Figure 2(a) shows the absorption spectra of the porphyrins recorded in tetrahydrofuran (THF) solution and on the film and corresponding data noted in Table 1. The porphyrins exhibit mainly two types of peaks. The intense sharp peaks at *ca*. 400-500 nm and weak peaks at *ca*. 500-700 nm are attributed to the Soret and Q-bands, respectively of the porphyrin macrocycle. The peaks at *ca*. 340-350 nm for ZnD(*p*-NI)PP are ascertained to localized transitions of the peripheral NI moiety. Impressively, the film of ZnD(*p*-NI)PP drop-casted from its THF solution becomes much more red-shifted and broadened than the film of ZnDPP. The results indicate that ZnD(*p*-NI)PP shows more typical end-to-end *J*-aggregates than ZnDPP.[10,18-20] The formation of *J*-aggregates for the porphyrins is useful to improve the light-harvesting, charge separation and transport charge carriers when employing them as a photocatalyst in PHE systems (*vide infra*).

Table 1. Photophysical and electrochemical data of ZnD(*p*-NI)PP and ZnDPP, and electron life time of ZnT(*p*-NI)PP.

Porphyrin	λ_{abs}/nm ($\varepsilon/10^4$)[a]	λ_{abs}/nm [b]	λ_{em} /nm[a]	λ_{em} /nm[b]	τ_F/ns [a]	(Φ_F) [a]	Φ_{ET}	E_{Ox}, V [c] (vs NHE)	E_{red}, V [d] (vs NHE)	$E_{0\text{-}0}$ /eV [e]
ZnD(*p*-NI)PP	353 (2.98), 342 (3.10) 413 (32.7), 544 (1.97), 583 (0.53)	361, 444, 569, 611	593, 640	610, 664	5.1	0.23	0.99	1.22, 1.59	– 0.78, – 1.16	2.23
ZnDPP	412 (2.34), 543 (0.18), 582 (0.02)	426, 548, 590	586, 635	604, 652	2.3	0.15	-	1.20, 1.56	– 0.77	2.20
ZnT(*p*-NI)PP	-		-		1.6	-		-	-	-

[a] THF solution. [b] Drop-casted thin films. [c] E_{ox} (vs NHE) = 0.77 + E_{ox} (vs Ferrocene). [c] E_{red} (vs NHE) = 0.77 – E_{red} (vs Ferrocene). [e] Estimated from the intersection of the normalized absorption and emission spectra.

Figure 3 shows the scanning electron microscope (SEM) and transmission electron microscope (TEM) images of the porphyrin films fabricated by the drop-cast method. The ZnDPP porphyrin self-assembled into microflower materials. In contrast, interestingly, the linear NI-substituted ZnD(*p*-NI)PP formed nanowires with length 1.5 to 5.0 μm (Figure S1) and width ranges from 100-250 nm (Figure S2). The TEM image of ZnD(*p*-NI)PP (Figure 3(e)) also clearly shows the nanowires morphology. Obviously, the linear *meso*-substituted NI moieties with typical stronger intermolecular interactions plays an important role in the nanowire self-assembly of ZnD(p-NI)PP. Nonetheless, developing of ZnD(*p*-NI)PP and comparing to ZnDPP represents a paradigm to

address the effect of NI moiety on the self-assembly of porphyrins and morphology, and consequently their application in PHE systems.

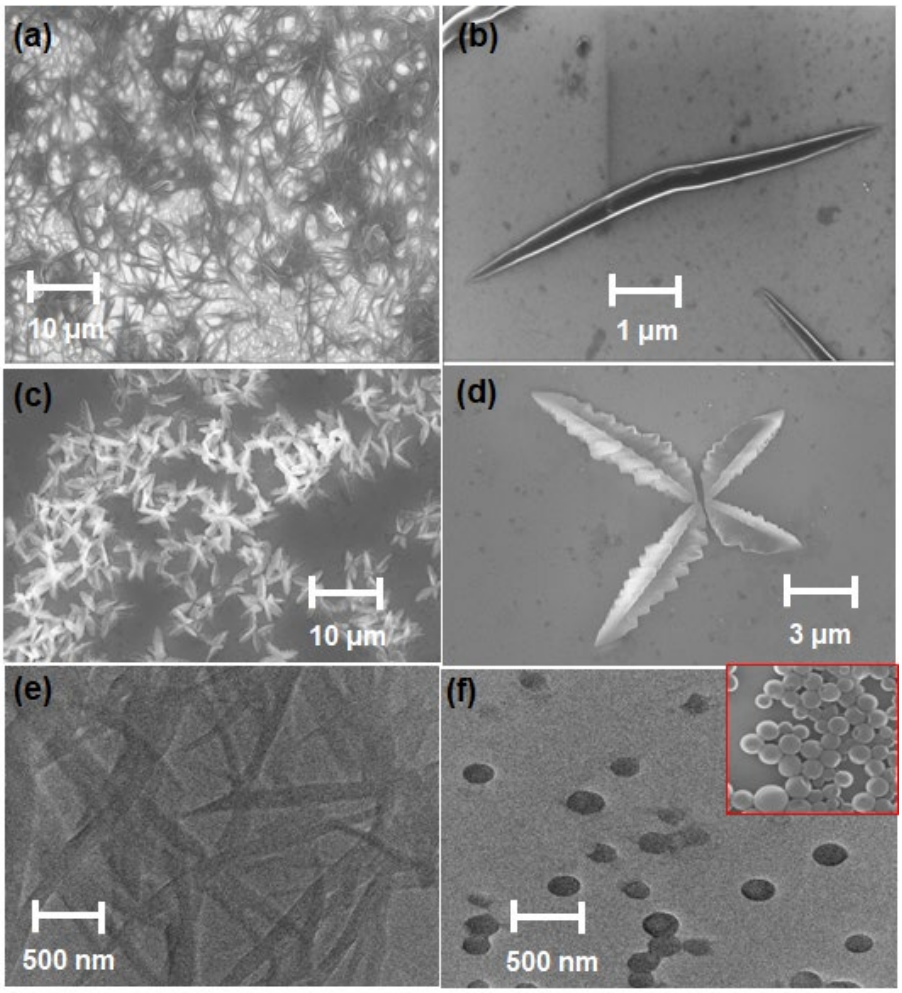

Figure 3. Typical SEM images of (a) and (b) ZnD(*p*-NI)PP, (c) and (d) ZnDPP, (e) Typical TEM image of ZnD(*p*-NI)PP and (f) Typical TEM image of ZnT(*p*-NI)PP (inset depicts SEM image). All the images were taken for drop-cast coated thin films of porphyrins from its THF solution (100 µM).

To further probe the morphology of porphyrins, we performed the powder X-ray diffraction (PXRD) analysis. All notable Bragg reflections were indexed (with offset of 0.0097° in 2θ) and

subsequently matched to the *P2/m* space group (Table S1). The diffraction pattern (Figure S3) of ZnD(*p*-NI)PP porphyrin yielded a monoclinic solution with lattice parameters of a = 4.7472(23) Å, b = 3.2025(10) Å, c = 2.8909(10) Å, β = 99.552(21)º and V = 43.34 Å^3. The figures of merit were M_7 = 162.3[21] and F_7 = 37.1 (0.0070, 27).[22] Note the sharp Bragg peaks at 18.92, 33.89, 33.95, 54.50, 54.66, 71.28, and 71.48˚ (2θ) corresponding to the (100), (110), $(10\overline{1})$, $(21\overline{1})$, (201), (220) and $(20\overline{2})$ crystalline planes, respectively, whereas ZnDPP porphyrin did not show any sharp peaks. It indicates that the ZnD(*p*-NI)PP porphyrin possesses highly crystallinity and the amorphous nature could be assigned to the ZnDPP. The crystalline nature of ZnD(*p*-NI)PP further reveals that the porphyrin molecules might be arranged in a perfect molecular ordering which could increase the mobility and transport of charge-carriers.[7] Thus it is meaningful to synthesize ZnD(*p*-NI)PP containing di-NI moieties for enhanced PHE (*vide infra*).

To gain insight on the effect of NI motif on the self-assembly of porphyrins, we further recorded SEM and TEM images of our recently reported ZnT(*p*-NI)PP porphyrin and well-known ZnTPP porphyrin without NI motif. As shown in Figure 3(f), S4 and S5, the ZnT(*p*-NI)PP porphyrin self-assembled into nanospheres with a particle size distribution from 150-300 nm (Figure S4), whilst the ZnTPP self-assembled into tetragonal microstructured materials (Figure S5). As ZnTPP porphyrin contains no NI motif, the self-assembly of ZnTPP was attested by the π–π stacking between the porphyrin rings of the neighboring molecules. Moreover, the morphology and size of the self-assembled materials of ZnTPP were completely different from that of tetra-NI conjugated ZnT(*p*-NI)PP porphyrin. All these results clearly speculate that the self-assembly process in ZnD(*p*-NI)PP porphyrin is not only induced by the π–π stacking between the porphyrin rings but also C=O···π and π···π interactions created by periphery NI moieties of the neighboring molecules.[12, 14, 15] This also further highlights that the porphyrins can be converted from amorphous

microflower to crystalline nanomaterials by simply attaching the NI moieties linearly to the *meso*-position of porphyrin ring rather than following conventional surfactant methods to prepare the porphyrin-based nanomaterials.[1, 2]

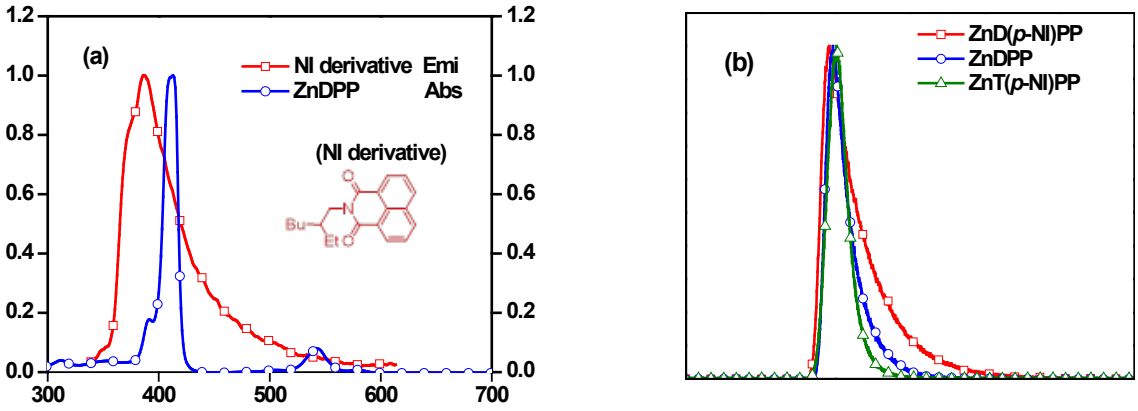

Figure 4. (a) The spectral overlap of the normalized fluorescence spectrum of NI derivative excited at 330 nm with the normalized absorption spectrum of ZnDPP and (b) Lifetime decay spectra of the porphyrins recorded in THF (10 μM) at room temperature.

As seen in Figure 2(b), both porphyrins show two emission peaks when excited at ca. 415 nm which corresponds to the absorption of the porphyrin ring Soret band. The strong peak at *ca*. 610–620 nm and a weaker one at *ca*. 650–680 nm originated from the porphyrin macrocycle. Obviously, ZnD(*p*-NI)PP exhibits strong emission peaks at *ca*. 610-680 nm under the excitation wavelength at *ca*. 330 nm which corresponds to NI chromophore absorption. Furthermore, the absence of emission peaks at *ca*. 360-380 nm corresponding to NI moiety indicates the most efficient intramolecular energy transfer (IET) between the NI energy donor and porphyrin ring energy acceptor in the ZnD(*p*-NI)PP porphyrin molecule. The intensity of ZnD(*p*-NI)PP emission peaks also increased when excited at 330 nm compared to that of 415 nm excitation. Therefore, it is also attesting the most efficient IET between NI and porphyrin macrocycle. The presence of IET is

reasonable due to an overlapped emission peak of NI derivative at an excitation of 330 nm with the Soret-band of ZnDPP (Figure 4(a)). The efficiency of energy transfer (Φ_{ET}) from NI substituents to the porphyrin ring of ZnD(*p*-NI)PP porphyrin was calculated according to our previous report.[17] The Φ_{ET} of ZnD(*p*-NI)PP was calculated to be 99% which is even higher than our earlier efficient ZnT(*p*-NI)PP porphyrin (92%). It indicates that conjugation of two NI moieties to the porphyrin ring is an ideal molecular design to achieve most efficient IET between NI moiety and porphyrin ring, consequently high fluorescence lifetime (τ_F) and quantum yield (Φ_F) (*vide infra*).

As seen from Figure 4(b), the lifetime (τ_F) of ZnD(*p*-NI)PP was recorded to be 5.1 ns which is over 2.2 and 3.2 fold higher than the ZnDPP (2.3 ns) and ZnT(*p*-NI)PP (1.6 ns), respectively. Impressively, the τ_F value of ZnD(*p*-NI)PP is superior to all star-shaped zinc porphyrins ever reported in the literature so far.[23-25] The Φ_F of ZnD(*p*-NI)PP was calculated to be 23% which is higher than the ZnDPP (15%) and ZnT(*p*-NI)PP (13%).[17] This is in agreement with their corresponding τ_F and Φ_{ET} values. The most efficient Φ_{ET} and superior τ_F value of ZnD(*p*-NI)PP than the ZnT(*p*-NI)PP suggest that conjugation of two NI energy donors to porphyrin energy acceptor in a linear-shaped molecular design is beneficial to achieve highly stabilized/long-lived photoexcited states of porphyrins. Consequently, it may improve the electron transfer from the excited porphyrins to the photo-catalyst (*vide infra*).

The redox potentials of the porphyrins were measured by performing cyclic voltammetry (CV) measurements (Figure S6). The ground-state oxidation potentials that corresponded to the HOMO levels of the porphyrins, ZnD(*p*-NI)PP and ZnDPP were calculated to be 1.22 and 1.20 V, respectively. And the calculated excited-state oxidation potentials (E_{ox}*) that corresponded to the LUMO levels are – 0.78 and – 0.77 V for ZnD(*p*-NI)PP and ZnDPP, respectively. The LUMO

energy levels of both porphyrins are more negative than the redox potential of H^+/H_2 (0 V vs. NHE) indicating that these porphyrins are suitable to be employed as photosensitizers in water reduction photocatalytic systems.

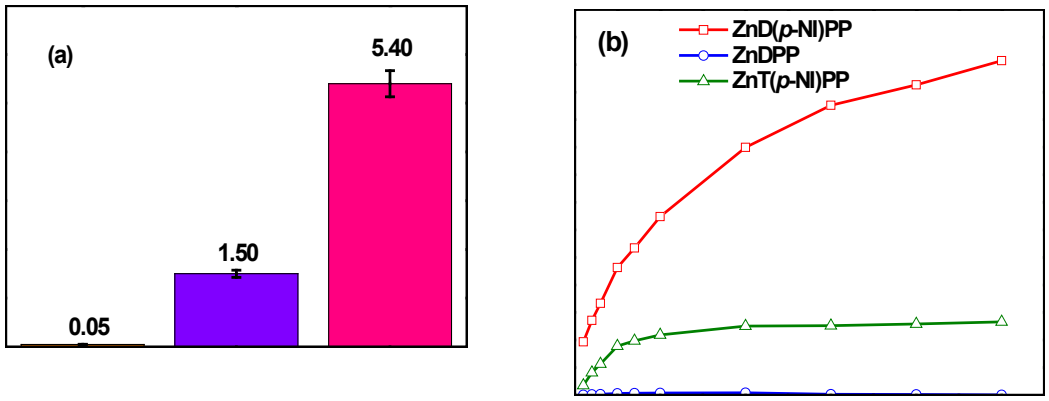

Figure 5. (a) H_2 production rate of photocatalytic systems under the irradiation for 5 h and (b) H_2 production of photocatalytic systems under the irradiation for 50 h: (Porphyrin (100 μM), Pt (3 wt %) and sacrificial donor/H_2O (1:9 v/v).

Table 2. H_2 production rate (ηH_2), apparent quantum efficiency (AQE) and turnover number (TON) data of photocatalytic systems.

Compound	ηH_2 (mmol g^{-1} h^{-1})[a]	TON[b]	AQE [c]
ZnD(*p*-NI)PP	5.40	62.50	1.40
ZnDPP	0.05	1.30	0.10
ZnT(*p*-NI)PP	1.50	24.80	0.40

[a,c] Calculated under irradiation for 5 h. [b] Calculated for 50 h

Since ZnD(*p*-NI)PP possesses good light-harvesting properties in majority of UV-Vis region in the solar spectrum, superior τ_F, suitable HOMO and LUMO energy levels, and forming well-

defined nanowires morphology with high crystallinity in solid, we employed it as a photocatalyst in heterogeneous PS and compared that with controlled ZnDPP porphyrin which lacks the NI moieties. The PHE results of the porphyrins are shown in Figure 5(a) and Table 2. The PS of ZnD(*p*-NI)PP exhibited higher H_2 production rate (ηH_2) of 5.4 mmol g^{-1} h^{-1} under the light irradiation of 5 h, which is over 108-fold higher than the ZnDPP (ηH_2 = 0.05 mmol g^{-1} h^{-1}). More interestingly, the ηH_2 of ZnD(*p*-NI)PP is also 3.6-fold higher than the ZnT(*p*-NI)PP (1.5 mmol g^{-1} h^{-1}).[17] The higher PHE results of linear-shaped di-NI conjugated porphyrin, ZnD(*p*-NI)PP compared to ZnDPP porphyrin could be explained by the following reasons: (i) high light-harvesting capability due to its broader UV-Vis spectra on the film; (ii) as ZnD(*p*-NI)PP contains highly stabilized excited states with longer τ_F, the transfer numbers of photo-excited electrons from the excited states of ZnD(*p*-NI)PP to Pt co-catalyst is high; and (iii) the crystalline nature of ZnD(*p*-NI)PP and high photocurrent response (*vide infra*) could improve the diffusion and transport of photoinduced charge carriers. The photostability of ZnD(*p*-NI)PP was tested by monitoring its PHE up to 50 h of irradiation time (Figure. 5(b)). Impressively, the ηH_2 of PS based on ZnD(*p*-NI)PP continuously increased and remained active up to 50 h from the initial time of irradiation, whereas the ηH_2 for the PSs of ZnDPP and ZnT(*p*-NI)PP increased up to 20 h and then dropped slowly after. It indicates that the linear-shaped di-NI substituted porphyrin, ZnD(*p*-NI)PP featuring nanowires morphology with an ordered molecular packing is highly photostable compared to the ZnDPP with microflowers morphology and star-shaped tetra-NI substituted porphyrin, ZnT(*p*-NI)PP with nanospheres morphology.

We also performed the reusability experiments to further confirm the stability and robustness of ZnD(*p*-NI)PP. As shown in Figure S7, the hydrogen production of ZnD(*p*-NI)PP appeared similar in each cycle of experiment indicating the ZnD(*p*-NI)PP is highly stable and possesses good

recycling ability. Moreover, the ηH_2 of linear-shaped porphyrin, ZnD(*p*-NI)PP is comparable to the most efficient porphyrin-based photocatalysts under heterogeneous basic condition reported yet.[26-28] In order to further confirm the stability of the solid-state morphology of porphyrins, SEM pictures of the photocatalytic systems containing porphyrins as photocatalysts irradiated after 5 h were recorded (Figure S8–S10). The morphology of SEM pictures of the photocatalytic systems remained similar to that of porphyrins drop-casted from its THF solution. These results strongly suggest that the self-assemblies of the porphyrins in solid state were induced by π-π stack interactions of both porphyrin and naphthalimide skeletons.

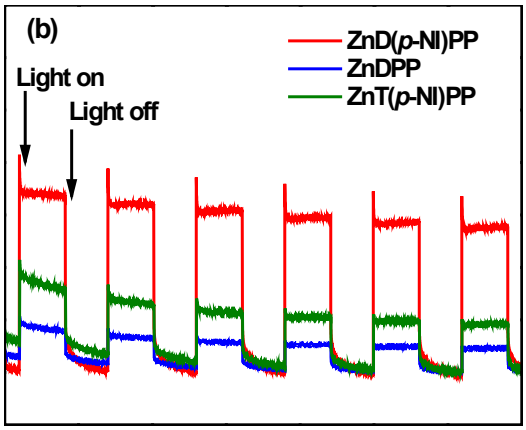

Figure 6. Photocurrent response spectra of the porphyrins.

To gain more insight into the photoinduced charge separation of ZnD(*p*-NI)PP, the transient photocurrent responses (i-t curves) studies were performed.[17, 29] As shown in Figure 6, the ZnD(*p*-NI)PP exhibited higher photocurrent response than ZnDPP and ZnT(*p*-NI)PP porphyrins indicating the efficient photogenerated hole-electron pairs separation and more electrons generated for the former porphyrin. This further attests its higher ηH_2 when it was employed as a photosensitizer. Moreover, the emission spectra and life decay spectra of PSs containing self-

assembled porphyrins were recorded to know the excited state properties of self-assembled porphyrin nanostructures (Figure S11 and S12). All of them are emissive and the emission wavelengths were red-shifted by *ca*. 20 nm compared to those of THF solution. Also, the red-shifted emission wavelengths of self-assembled ZnDPP and ZnD(*p*-NI)PP porphyrins are consistent with their drop-casted thin films emission wavelengths. The lifetime (τ_F) of ZnD(*p*-NI)PP self-assemblies was recorded to be 1.6 ns which is over 2.0 fold higher than the ZnDPP (0.8 ns) and ZnT(*p*-NI)PP (0.9 ns) self-assembles, respectively. The higher τ_F of ZnD(*p*-NI)PP self-assemblies than the ZnDPP and ZnT(*p*-NI)PP self-assemblies also supports that the ZnD(*p*-NI)PP self-assembled nanowires possess highly stabilized excited states, thus efficient charge separation and transfer of excited electrons to the Pt co-catalyst where proton reduction occurs. Finally, all these results demonstrate that the linear 5,15-substituted NI porphyrin, ZnD(*p*-NI)PP featuring nanowires morphology with more orderly molecular packing is more beneficial than the ZnDPP and ZnT(*p*-NI)PP with microflowers and nanospheres, respectively, in terms of morphology to improve the PHE and photostability via enhancing the light-harvesting property, stabilizing photoexcited state with efficient electron-hole separation, consequently, transporting electrons to Pt co-catalyst where the proton reduction occurs.

CONCLUSIONS

In summary, we synthesized a new porphyrin derivative ZnD(*p*-NI)PP with linear 5,15-substituted naphthalimide (NI) moieties and compared its photophysical, morphological and PHE properties with ZnDPP without NI moieties. Optoelectronic and photocurrent response studies revealed that the ZnD(*p*-NI)PP possessed higher light-harvesting properties and more efficient photogenerated electron-hole separation, more stabilized photo-excited states with higher τ_F and Φ_F than ZnDPP. The morphology analyses demonstrated that the ZnD(*p*-NI)PP self-assembled into crystalline

nanowires, while microflowers and amorphous nature assigned to ZnDPP. As a result, the ZnD(*p*-NI)PP delivered a ηH_2 of 5.4 mmol g^{-1} h^{-1}, which is over 108-fold higher than the ZnDPP (ηH_2 = 0.05 mmol g^{-1} h^{-1}), and 3.6-fold higher than the ZnT(*p*-NI) (ηH_2 = 1.5 mmol $g^{-1}h^{-1}$) which bears four NI units and self-assembled into nanospheres in solid. Also, the ZnD(*p*-NI)PP is highly photostable and continued to show ηH_2 up to 50 h, whereas ZnDPP dropped in ηH_2 after 20 h. The high PHE performance of ZnD(*p*-NI)PP could be attributed to the highly stabilized photo-excited states, efficient photogenerated charge carriers separation and transport which further enhanced the electron transfer from the photo-excited porphyrin moiety to the Pt co-catalyst where proton reduction takes place.

METHODS

Preparation of photocatalytic systems. A multichannel photochemical reaction system fixed with OLED white light (PCX50B, 148.5 mW/cm^2) was used as the light source. The photocatalytic hydrogen (H_2) evolution experiments were performed in a quartz vial reactor (20 mL) sealed with a rubber septum, gas-closed system, at ambient temperature and pressure Initially, the prepared sample powder (0.1 mM) was suspended in aqueous triethanolamine (TEOA)/Water = 1 : 9 v/v) under constant stirring. Then, 3 wt.% of Pt as co-catalyst was loaded by in situ photoreduction deposition method, H_2PtCl_6 aqueous as Pt source. The suspension was purged with nitrogen gas for 30 min to ensure anaerobic conditions and then it was placed at the position of 15 cm away from lamp. After 1h irradiation, the released gas (400 μL) was collected by syringe from the headspace of the reactor and was analyzed by gas chromatography (Shimadzu, GC-2014, Japan, with ultrapure Ar as a carrier gas) equipped with a TDX-01(5 Å molecular sieve column) and a thermal conductivity detector (TCD). Eventually, the total content of photocatalytic H_2 evolution was calculated according to the standard curve. Continuous stirring was applied to the whole

process to keep the photocatalyst particles in suspension state and get the uniform irradiation. The stability of the photocatalytic systems were investigated by measuring the ηH_2 over 50 hours.

The apparent quantum efficiency (AQE) was measured under the similar photocatalytic reaction conditions except using 420 nm OLED light. The focused intensity and illuminated area LED light were ca. 68.0 mW/cm^2 and 9.04 cm^2, respectively. AQE was calculated via the following equation:

$$\text{AQE} = \left(\frac{2 \times \text{number of hydrogen molecules}}{\text{number of incident photons}}\right) \times 100\%$$

The turnover number (TON) was calculated after 1 hour by using the following formula;

$$\text{TON} = \frac{\text{Number of moles of hydrogen produced in photocatalytic system}}{\text{Number of moles of photocatalyst}}$$

Photoelectrochemical Measurement. The photoelectrochemical tests were performed according to our recent report.[29]

Supporting Information

Supporting Information file contains the following contents: materials and methods, synthesis, SEM and TEM images, size distribution analysis, cyclic voltammograms, ^{1}H and ^{13}C NMR spectra, and MALDI–TOF spectrum.

AUTHOR INFORMATION

Corresponding Author

* X. Zhu, E-mail: xjzhu@hkbu.edu.hk

* Wai-Yeung Wong: wai-yeung.wong@polyu.edu.hk

Notes

There are no conflicts to declare.

ACKNOWLEDGMENT

This work was supported by the Australia Research Council (ARC) (DP180104010), Hong Kong Baptist University (FRG2-17-18-068, RC-ICRS/15-16/02E, RC-ICRS/1617/02C-CHE, RC-ICRS-18-19-01A, RC-IRMS/16/17/02CHEM). W.-Y.W. thanks the financial support from the Hong Kong Research Grants Council (C4006-17G and PolyU 123384/16P), the Hong Kong Polytechnic University (1-ZE1C) and Ms. Clarea Au for the Endowed Professorship in Energy (847S).

REFERENCES

1. Li, Q.; Zhao, N.; Bai, F. Size- and Shape-dependent Photocatalysis of Porphyrin Nanocrystals. *MRS Bulletin* **2019**, *44*, 172-177.

2. Chen, Y.; Li, A.; Huang, Z.-H.; Wang, L.-N.; Kang, F. Porphyrin-Based Nanostructures for Photocatalytic Applications. *Nanomaterials* **2016**, *6*, 51.

3. Zhou, X.; Tang, W.; Bi, P.; Yan, L.; Wang, X.; Wong, W.-K.; Hao, X.; Ong, B. S.; Zhu, X. Chemically Driven Supramolecular Self-assembly of Porphyrin Donors for High-performance Organic Solar Cells. *J. Mater. Chem. A* **2018**, *6*, 14675-14680.

4. Armaroli, N.; Balzani, V. The Future of Energy Supply: Challenges and Opportunities. *Angew. Chem., Int. Ed*. **2007**, *46*, 52-66.

5. Zhao-Karger, Z.; Gao, P.; Ebert, T.; Klyatskaya, S.; Chen, Z.; Ruben, M.; Fichtner, M. New Organic Electrode Materials for Ultrafast Electrochemical Energy Storage. *Adv. Mater.* **2019**, *31*, 1806599.

6. Zhang, N.; Wang, L.; Wang, H.; Cao, R.; Wang, J.; Bai, F.; Fan, H. Self-Assembled One-Dimensional Porphyrin Nanostructures with Enhanced Photocatalytic Hydrogen Generation. *Nano Lett.* **2018**, *18*, 560-566.

7. Wang, Y.; Sun, L.; Wang, C.; Yang, F.; Ren, X.; Zhang, X.; Dong, H.; Hu, W. Organic Crystalline Materials in Flexible Electronics. *Chem. Soc. Rev*. **2019**, *48*, 1492-1530.

8. Jiang, Y.-B.; Sun, Z. Self-assembled Porphyrin and Macrocycle Derivatives: From Synthesis to Function. *MRS Bulletin* **2019**, *44*, 167-171.

9. Shirakawa, M.; Kawano, S.-i.; Fujita, N.; Sada, K.; Shinkai, S., Hydrogen-Bond-Assisted Control of H versus J Aggregation Mode of Porphyrins Stacks in an Organogel System. *J. Org. Chem*. **2003**, *68*, 5037-5044.

10. Pandey, R. K.; Chitgupi, U.; Lakshminarayanan, V., Porphyrin Aggregates in the form of Nanofibers and their Unusual Aggregation Induced Emission. *J. Porphyr. Phthalocyanines* **2012**, *16*, 1055-1058.

11. Ladomenou, K.; Natali, M.; Iengo, E.; Charalampidis, G.; Scandola, F.; Coutsolelos, A. G., Photochemical Hydrogen Generation with Porphyrin-based Systems. *Coord. Chem. Rev.* **2015**, *304-305*, 38-54.

12. Kitchen, J. A.; Martinho, P. N.; Morgan, G. G.; Gunnlaugsson, T. Synthesis, Crystal Structure and EPR Spectroscopic Analysis of Novel Copper Complexes Formed from N-pyridyl-4-nitro-1,8-naphthalimide ligands. *Dalton Trans*. **2014**, *43*, 6468-6479.

13. Reger, D. L.; Horger, J. J.; Smith, M. D. Copper(ii) Carboxylate Tetramers Formed from an Enantiopure Ligand Containing a π-stacking Supramolecular Synthon: Single-Crystal to Single-Crystal Enantioselective Ligand Exchange. *Chem. Commun.* **2011**, *47*, 2805-2807..

14. Pagidi, S.; Kalluvettukuzhy, N. K.; Thilagar, P. Tunable Self-Assembly and Aggregation-Induced Emission Characteristics of Triarylboron-Decorated Naphthalimides. *Organometallics* **2018**, *37*, 1900-1909.

15. Meher, N.; Iyer, P. K., Spontaneously Self-Assembled Naphthalimide Nanosheets: Aggregation-Induced Emission and Unveiling a-PET for Sensitive Detection of Organic Volatile Contaminants in Water. *Angew. Chem., Int. Ed*. **2018**, *57*, 8488-8492.

16. Şahin Ün, Ş.; Zehra Topal, S.; Zorlu, Y. Naphthalimide-cyclophosphazene Combination: Synthesis, Crystal Structure, Photophysics and Solid-state Fluorescence. *J. Lumin*. **2017**, *190*, 23-28.

17. Bodedla, G. B.; Li, L.; Che, Y.; Jiang, Y.; Huang, J.; Zhao, J.; Zhu, X. Enhancing Photocatalytic Hydrogen Evolution by Intramolecular Energy Transfer in Naphthalimide Conjugated Porphyrins. *Chem. Commun*. **2018***, 54*, 11614-11617.

18. Yamaguchi, T.; Kimura, T.; Matsuda, H.; Aida, T. Macroscopic Spinning Chirality Memorized in Spin-Coated Films of Spatially Designed Dendritic Zinc Porphyrin J-Aggregates. *Angew. Chem., Int. Ed.* **2004**, *43*, 6350-6355.

19. Maiti, N. C.; Mazumdar, S.; Periasamy, N. J- and H-Aggregates of Porphyrin-Surfactant Complexes: Time-Resolved Fluorescence and Other Spectroscopic Studies. *J. Phys. Chem. B* **1998**, *102*, 1528-1538.

20. Morisue, M.; Morita, T.; Kuroda, Y. Ligand-assisted J-type Aggregates of Zinc Porphyrin: Anticooperative Molecular Organization in Self-assembled Bolaamphiphile. *Org. Biomol. Chem.* **2010**, *8*, 3457-3463.

21. De Wolff, P. M. A simplified Criterion for the Reliability of A Powder Aattern Indexing. *J. Appl. Cryst*. **1968**, ***1***, 108-113.

22. Smith, G. S.; Snyder. R. L. A Criterion for Rating Powder Diffraction Patterns and Evaluating the Reliability of Powder-pattern Indexing**.** *J. Appl. Cryst*. **1968**, *121*, 60-65.

23. Rananaware, A.; Bhosale, R. S.; Ohkubo, K.; Patil, H.; Jones, L. A.; Jackson, S. L.; Fukuzumi, S.; Bhosale, S. V.; Bhosale, S. V. Tetraphenylethene-Based Star Shaped Porphyrins: Synthesis, Self-assembly, and Optical and Photophysical Study. *J. Org. Chem*. **2015**, *80*, 3832-3840.

24. Leonardi, M. J.; Topka, M. R.; Dinolfo, P. H. Efficient Förster Resonance Energy Transfer in 1,2,3-Triazole Linked BODIPY-Zn(II) Meso-tetraphenylporphyrin Donor-Acceptor Arrays. *Inorg. Chem*. **2012**, *51*, 13114-13122.

25. Rajesh, C. S.; Capitosti, G. J.; Cramer, S. J.; Modarelli, D. A. Photoinduced Electron-Transfer within Free Base and Zinc Porphyrin Containing Poly(Amide) Dendrimers. *J. Phys. Chem. B* **2001**, *105*, 10175-10188.

26. Zhu, M.; Li, Z.; Xiao, B.; Lu, Y.; Du, Y.; Yang, P.; Wang. X. Surfactant Assistance in Improvement of Photocatalytic Hydrogen Production with the Porphyrin Noncovalently Functionalized Graphene Nanocomposite, *ACS Appl. Mater. Interfaces*. **2013**, *5*, 1732-1740

27. Mei, S.; Gao, J.; Zhang, Y.; Yang, J.; Wu, Y.; Wang, X.; Zhao, R.; Zhai, X.; Hao, C.; Li, R.; Yan, J. Enhanced Visible Light Photocatalytic Hydrogen Evolution Over Porphyrin Hybridized Graphitic Carbon Nitride, *J. Colloid Interface Sci.* **2017**, *506*, 58-65

28. Li, H.; Jie, L.; Pan, J.; Kang, L.; Yao, J. Direct Photocatalytic Hydrogen Evolution from Water Splitting Using Nanostructures of Hydrate Organic Small Molecule as Photocatalysts, *J. Mater. Chem. A* **2016**, *4*, 6577-6584.

29. Tritton, D. N.; Bodedla, G. B.; Tang, G.; Zhao, J.; Kwan, C.-S.; Leung, K. C.-F.; Wong, W.-Y.; Zhu, X. *J. Mater. Chem. A* **2020**, *8*, 3005-3010.

Table of Contents

A linear naphthalimide substituted porphyrin, ZnD(*p*-NI)PP self-assembles into nanowires and shows higher efficiency and stability in photocatalytic hydrogen evolution than the porphyrin without naphthalimide (ZnDPP) as microflowers in solid.

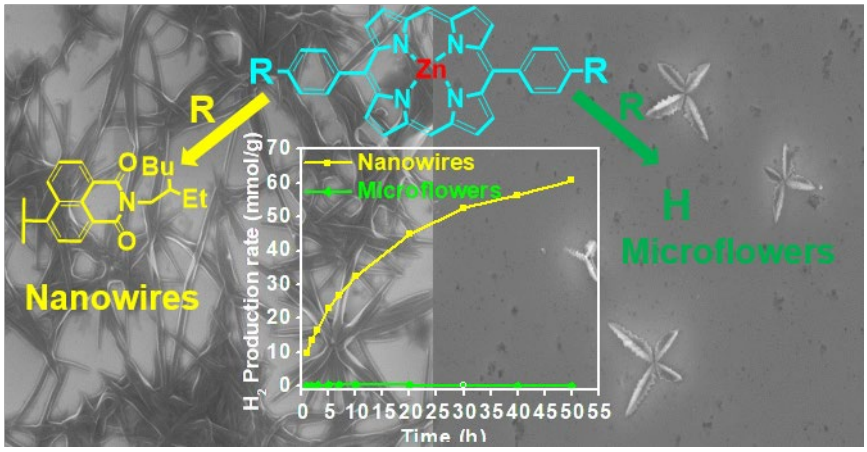
R
R
R
N
Zn
N
N
N
O
Bu
N
Et
O
Nanowires
H
Microflowers
Nanowires
Microflowers
H2 Production rate (mmol/g)
70
60
50
40
30
20
10
0
0 5 10 15 20 25 30 35 40 45 50 55
Time (h)